Pergamon

Int. J. Solids Structures Vol. 33, No. 26, pp. 3903–3923, 1996

0020-7683/96 $15.00 + .00

0020-7683(95)00222-7

ANALYSIS OF PLASTIC BUCKLING OF STEEL PLATES IN SHEAR BASED ON THE TRESCA YIELD CRITERION

TETSURO INOUE
Institute of Engineering Mechanics, University of Tsukuba, Tsukuba, Japan

(*Received* 12 *January* 1995; *in revised form* 7 *September* 1995)

Abstract—Plasticity in steel is characterized by an appreciable amount of plastic flow (in the yield plateau range) which precedes strain hardening. The plastic behavior of materials is most pronounced in the material with plastic flow such as mild steel. The author has previously (1993 and 1994) proposed a new idea of the role of plastic flow in the plastic plate buckling under uniaxial compression [Inoue, T. and Kato, B. (1993). Analysis of plastic buckling of steel plates. *Int. J. Solids Structures* **30**, 835–856; Inoue, T. (1994). Analysis of plastic buckling of rectangular steel plates supported along their four edges. *Int. J. Solids Structures* **31**, 219–230]. The original idea was to find a new torsional mode of plates which had not been noticed by anyone at the instant of buckling. The new mode was based on the concept that plastic strain was created by slips based on the Tresca yield criterion, and gave a significant reduction of the shear modulus. Its analytical solutions for the plastic buckling were compared with test results, and a good agreement in the early plastic zone was obtained. This paper aims to solve analytically the plastic buckling stress of mild steel plates in shear based on the similar concept adopted in the previous papers. Copyright © 1996 Elsevier Science Ltd.

1. INTRODUCTION

Analysis of plastic buckling of plates has a long historical background. Representative investigations for plates in shear were published by Gerard (1948), Stowell (1949) and Bijlaard (1949). In these investigations, Gerard suggested the secant modulus method, and Stowell and Bijlaard employed deformation theory for the analysis of plastic buckling of plates. The very close solutions were derived by the above two procedures. The deformation theory gives lower solutions than test results of mild steel plates under uniaxial compression. It is not rational for the problem of plate buckling because stress bifurcates from proportional loading. On the other hand, it is well known that incremental theory, which seems to be rational, gives higher solutions for plastic buckling stress than test results. The discrepancy between theoretical value and test results was diminished by recent investigations (Sewell, 1973 and 1974, Inoue and Kato, 1993 and Inoue, 1994) in the case of uniaxial compression. Shear buckling is not, however, treated there. Historical reviews of investigations for plastic plate buckling were summarized by the author (Inoue and Kato, 1993).

The author has already developed a creative study of plastic buckling of steel plates under uniaxial compression. In its analysis yielding of steel plate was to follow the Tresca yield criterion. Plastic deformation of the plate was to be caused by slips which developed only in the directions of maximum shear stress. The author has found there a new buckling mode and significantly reduced shear modulus which had not been noticed previously. Theoretically obtained buckling strength has been in good agreement with test results, especially in the early plastic zone.

In this paper, buckling stress of simply supported rectangular steel plates in shear is theoretically obtained. It is assumed, similarly to the previous investigation (Inoue and Kato, 1993), that yielding follows the Tresca yield criterion and plastic deformation is to be caused by slips which develop only in the direction of maximum shear stress. Evaluation of bending and torsional stiffnesses becomes a problem in the analysis of plastic plate buckling. These are derived under the condition that any strain reversal is not created at the instant of plastic buckling. This concept was established as tangent modulus theory by

Shanley (1947), and was applied to the plastic buckling analysis of plate based on deformation theory by Stowell (1948 and 1949). In this paper, obtained bending stiffnesses have the same values even in the plastic flow and strain hardening ranges as those in the elastic range, and torsional stiffness vanishes in the plastic flow range and is expressed by the use of tangent modulus on the shear stress–strain curve in the strain hardening range.

The difference between the author's analysis and that of incremental theory is described in the Appendix.

2. BENDING AND TORSIONAL STIFFNESSES IN THE PLASTIC RANGE

2.1. *Relation between the stress and strain increments*

Yielding is assumed to follow the Tresca yield criterion and the plastic deformation is generated by planar slipping in the direction of maximum shear stress. This assumption tacitly includes the fact that the enlarged yield locus keeps similarity to the initial shape of yield locus. The plastic strain increment of yielded steel plates in shear contains only shear strain components even if any strain reversal is not created. Therefore, the increment of normal strain is perfectly elastic in both plastic flow and strain hardening ranges. The shear modulus is zero in the plastic flow range because the increment of shear strain takes place indefinitely without any stress increase in shear. In the strain hardening range, the shear modulus is uniquely expressed by the use of the hardening modulus E_t of the coupon test if E_t is constant throughout the plastic range. It is suitable to relate the increment of maximum shear stress $d\tau_{max}$ with the increment of maximum plastic shear strain $d\gamma_{max}$ under the Tresca yield criterion. So, to find the relation above, the property revealed by uniaxial tension is applicable. When the direction of uniaxial tension coincides with the x-axis, there is the following relation among each increment of principal plastic strain.

$$d\varepsilon_x^p = -2\,d\varepsilon_y^p = -2\,d\varepsilon_z^p \tag{1}$$

where

$d\varepsilon_x^p$ = increment of plastic principal strain in the x direction
$d\varepsilon_y^p$ = increment of plastic principal strain in the y direction
$d\varepsilon_z^p$ = increment of plastic principal strain in the z direction.

The increment of maximum plastic shear strain which corresponds to eqn (1) is given by

$$d\gamma_{max}^p = \frac{3}{2}\,d\varepsilon_x^p = \frac{3}{2}\left(d\varepsilon_x - \frac{d\sigma_x}{E}\right) \tag{2}$$

where

$E = 2.059 \times 10^5$ N mm^{-2} = Young's modulus
$d\gamma_{max}^p$ = increment of maximum plastic shear strain
$d\varepsilon_x$ = increment of normal strain in the x direction under uniaxial tension, and equal to $d\varepsilon_x^p$ in the plastic flow range
$d\sigma_x$ = increment of normal stress in the x direction under uniaxial tension, which vanishes in the plastic flow range.

The increment of maximum shear stress is given by

$$d\tau_{max} = \tfrac{1}{2}\,d\sigma_x \tag{3}$$

where

$d\tau_{max}$ = increment of maximum shear stress which vanishes in the plastic flow range

There is the following relation in uniaxial tension

$$d\sigma_x = E_t\, d\varepsilon_x \tag{4}$$

where

E_t = tangent modulus.

In the strain hardening range eqns (2)–(4) give

$$d\gamma^p_{max} = 3\left(\frac{1}{E_t} - \frac{1}{E}\right)d\tau_{max}. \tag{5}$$

In the plastic flow range, there is the following relation

$$d\gamma^p_{max} = d\kappa \tag{6}$$

where

$d\kappa$ = positive indefinite scalar

In the strain hardening range, adding the elastic component to eqn (5), the following equation is obtained

$$d\gamma_{max} = \left[\frac{1}{G} + 3\left(\frac{1}{E_t} - \frac{1}{E}\right)\right]d\tau_{max} \tag{7}$$

where

$d\gamma_{max}$ = increment of maximum shear strain

$G = E/2(1+\nu)$ = elastic modulus in shear

$\nu = 0.3$ = Poisson's ratio of steel.

Figure 1 shows a plate in shear with working stress expressed by arrows. Directions of x- and y-axes are defined anew as Fig. 1. The directions of maximum shear stress and strain coincides with x- and y-axes. Therefore eqns (6) and (7) can be applied to those directions.

Bringing the above consideration to a conclusion.

(a) Plastic flow range

$$\left.\begin{aligned} d\varepsilon_x &= \frac{1}{E}(d\sigma_x - \nu\, d\sigma_y) \\ d\varepsilon_y &= \frac{1}{E}(d\sigma_y - \nu\, d\sigma_x) \\ d\gamma_{xy} &= d\kappa \end{aligned}\right\} \tag{8}$$

where

$d\varepsilon_x$, $d\varepsilon_y$ = increment of normal strain in the x and y axis respectively

$d\sigma_x$, $d\sigma_y$ = increment of normal stress in the x and y axis respectively

$d\gamma_{xy}$ = increment of shear strain in the xy component.

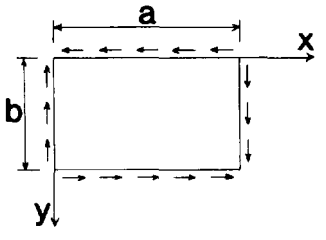

Fig. 1. Direction of axes and working shear stress.

(b) Strain hardening range

$$\left.\begin{aligned} \mathrm{d}\varepsilon_x &= \frac{1}{E}(\mathrm{d}\sigma_x - \nu\,\mathrm{d}\sigma_y) \\ \mathrm{d}\varepsilon_y &= \frac{1}{E}(\mathrm{d}\sigma_y - \nu\,\mathrm{d}\sigma_x) \\ \mathrm{d}\gamma_{xy} &= \left[\frac{1}{G} + 3\left(\frac{1}{E_t} - \frac{1}{E}\right)\right]\mathrm{d}\tau_{xy} \end{aligned}\right\} \tag{9}$$

where $\mathrm{d}\tau_{xy}$ = increment of shear stress in the xy component.

2.2. *Bending and torsional stiffness in the plastic flow range*

The bending and torsional moments of orthogonally anisotropic plate are generally expressed by the following equation.

$$\left.\begin{aligned} M_x &= D_x I\phi_x + D_{xy} I\phi_y \\ M_y &= D_{yx} I\phi_x + D_y I\phi_y \\ M_{xy} &= 2G_p I\phi_{xy} \end{aligned}\right\} \tag{10}$$

where

$I = t^3/12$

t = thickness of a plate

$D_x I$, $D_y I$, $D_{xy} I$, $D_{yx} I$ = bending stiffnesses

$G_p I$ = torsional stiffness

G_p = shear modulus

$\phi_x = -\partial^2 w/\partial x^2$ = curvature in the x direction

$\phi_y = -\partial^2 w/\partial y^2$ = curvature in the y direction

$\phi_{xy} = \partial^2 w/\partial x\,\partial y$ = twist of the surface with respect to the x- and y-axes

w = out-of-plane displacement of the plate.

Directions of bending and torsional moments which work on a plate element are defined by Fig. 2.

(a) Bending stiffnesses in the plastic flow range

Because increments of normal strain $\mathrm{d}\varepsilon_x$ and $\mathrm{d}\varepsilon_y$ of yielded plates in shear created by buckling are perfectly elastic by eqn (8), all the bending stiffnesses take elastic values. Therefore these values are given as follows:

$$\left.\begin{aligned} D_x I = D_y I &= \frac{E}{1-\nu^2} I \\ D_{xy} I = D_{yx} I &= \frac{\nu E}{1-\nu^2} I \end{aligned}\right\} \tag{11}$$

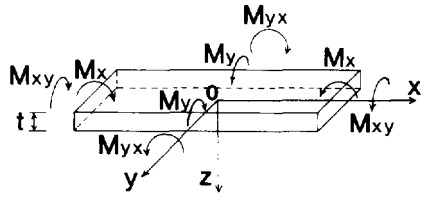

Fig. 2. Direction of moment.

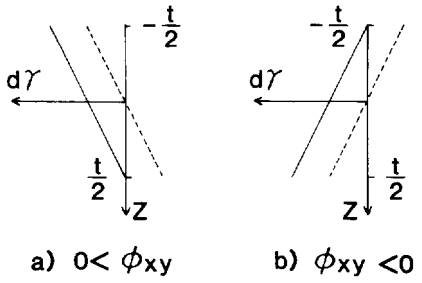

Fig. 3. Distribution of shear strain.

(b) Torsional stiffness in the plastic flow range

The distribution of the increment of shear strain accompanied by torsional deformation at the instant of buckling is assumed to be linear to the direction of plate thickness. This assumption is true in the elastic buckling, and the distribution is given by

$$d\gamma_{xy} = -2z\phi_{xy} \tag{12}$$

where z = axis along the plate thickness with an origin at the center of plate thickness.

The increments of shear strain given by eqn (12) are expressed by dashed lines in Fig. 3(a), (b) for positive ϕ_{xy} and negative ϕ_{xy}, respectively. The condition that any strain reversal is not be created at the instant of plastic buckling is satisfied by the progression of the average shear strain at the center of plate thickness. Then we obtain

$$d\gamma_{xy} = \beta - 2z\phi_{xy} \tag{13}$$

where β = average increment of shear strain which progresses at the center of plate thickness.

When the direction of working shear stress coincides with positive direction of $d\gamma_{xy}$, β is positive. Then, the distributions of the increment of shear strain given by eqn (13) are illustrated by solid lines in Fig. 3. This figure shows the two limit states in which the condition of no strain reversal is just satisfied by the condition that the increment of shear strain of right or reverse side of the plate remains zero. When the working shear stress takes opposite direction of $d\gamma_{xy}$, it is suitable to consider β is negative.

The progression of $d\gamma_{xy}$ in eqn (8) is brought about without any increase of shear stress. Therefore, the shear modulus in this range is given by

$$G_p = 0 \tag{14}$$

Thus torsional stiffness in eqn (10) is also zero.

(c) Bending stiffness in the strain hardening range

All the bending stiffnesses take the elastic values and are given by eqn (11), similarly to those in plastic flow range because eqn (9) means $d\varepsilon_x$ and $d\varepsilon_y$ are elastic.

(d) Torsional stiffness in the strain hardening range

The distributions of the increment of shear strain accompanied by torsional deformation at the instant of buckling are considered to be similar to those of plastic flow range. Therefore these are again illustrated by solid lines in Fig. 3. In this case, the relation between the increments of shear stress and strain is expressed by eqn (9). As a result, I obtain the following shear modulus:

$$G_p = \frac{1}{\frac{1}{G} + 3\left(\frac{1}{E_t} - \frac{1}{E}\right)} \tag{15}$$

Thus torsional stiffness is obtained by multiplying I by G_p.

3. BUCKLING OF RECTANGULAR STEEL PLATES IN SHEAR

The boundary condition around the plates treated in this paper is simply supported.

3.1. *Elastic buckling of rectangular steel plates in shear*

Stein and Neff (1947) has solved this problem by calculating a 10 order determinant. There is a precise solution by Seydel (1933) for a plate whose aspect ratio $\alpha(=a/b$, b and a: breadth and length of a plate, respectively) is equal to 1. And there is another precise solution by Southwell and Scan (1924) for a long plate ($\alpha = \infty$). Southwell and Scan had obtained the buckling stress by analyzing the free oscillation of the plate. Namely, they had found out the buckling stress at which its frequency vanishes. Based on the above results, Bleich (1952) derived an approximate parabola as follows taking $1/\alpha$ as a parameter for the range $0 \leqslant 1/\alpha \leqslant 1$.

$$\tau_{cr} = \frac{\pi^2 E}{12(1-\nu^2)}\left(\frac{t}{b}\right)^2 Ke \tag{16}$$

$$Ke = 5.34 + 4\left(\frac{1}{\alpha}\right)^2 \tag{17}$$

(apply for $\alpha \geqslant 1$)

where τ_{cr} = buckling shear stress

For $\alpha < 1$ there is the following conversion

$$\tau_{cr} = \frac{\pi^2 E}{12(1-\nu^2)}\left(\frac{t}{a}\right)^2 K'\left(\frac{b}{b}\right)^2 = \frac{\pi^2 E}{12(1-\nu^2)}\left(\frac{t}{b}\right)^2 K'\left(\frac{b}{a}\right)^2 \tag{18}$$

where K' = value of K_c obtained by substituting $1/\alpha$ instead of α in eqn (17).

Therefore we obtain

$$K_c = K'\left(\frac{b}{a}\right)^2 = 4.0 + 5.34\left(\frac{1}{\alpha}\right)^2 \tag{19}$$

(apply for $\alpha < 1$).

3.2. *Plastic buckling of rectangular steel plates in shear*

In this section, yielded steel plates are considered to be orthogonally anisotropic plates. Their buckling stresses are estimated approximately by energy method. Sectional stiffnesses derived in Section 2 are utilized in the analysis.

(a) When α has a finite value.

Buckling mode can be expressed by the following Fourier series when all edges are simply supported.

$$w = \sum_{m=1}^{\infty}\sum_{n=1}^{\infty} f_{mn} \sin\frac{m\pi}{a}x \sin\frac{n\pi}{b}y \tag{20}$$

x- and y-axes are defined in Fig. 1.

The buckling stress is obtained by the following procedure. Firstly, set the strain energy created by buckling equal to the work of external forces. Secondly obtain the buckling stress by the condition to minimize it. This procedure is similar to the elastic buckling analysis by Timoshenko and Gere (1961).

The strain energy V of orthogonally anisotropic plates is expressed by the following equation.

$$V=\tfrac{1}{2}I\int\int\left[D_x\left(\frac{\partial^2 w}{\partial x^2}\right)^2+D_y\left(\frac{\partial^2 w}{\partial y^2}\right)^2+(D_{xy}+D_{yx})\frac{\partial^2 w}{\partial x^2}\cdot\frac{\partial^2 w}{\partial y^2}+4G_p\left(\frac{\partial^2 w}{\partial x\,\partial y}\right)^2\right]\mathrm{d}x\,\mathrm{d}y \tag{21}$$

Integrating the eqn (21), we obtain

$$V=\frac{ab}{8}I\sum_{m=1}^{\infty}\sum_{n=1}^{\infty}f_{mn}^2\left[D_x\left(\frac{m^2\pi^2}{a^2}\right)^2+D_y\left(\frac{n^2\pi^2}{b^2}\right)^2+(D_{xy}+D_{yx})\frac{m^2n^2\pi^4}{a^2b^2}+4G_p\frac{m^2n^2\pi^4}{a^2b^2}\right] \tag{22}$$

The work T of external forces is expressed by

$$T=-{}_{cr}N_{xy}\int\int\frac{\partial w}{\partial x}\cdot\frac{\partial w}{\partial y}\mathrm{d}x\,\mathrm{d}y \tag{23}$$

where ${}_{cr}N_{xy}=\tau_{cr}t$ = shear buckling strength per unit width.

Integrating eqn (23) we obtain

$$T=-4{}_{cr}N_{xy}\sum_m\sum_n\sum_p\sum_q f_{mn}f_{pq}\frac{mnpq}{(m^2-p^2)(q^2-n^2)} \tag{24}$$

where m, n, p and q = integers which made $m\pm p$ and $n\pm q$ odd numbers.

By eqns (22) and (24), ${}_{cr}N_{xy}$ is obtained as the following.

$${}_{cr}N_{xy}=-\frac{abI}{32}\frac{\displaystyle\sum_{m=1}^{\infty}\sum_{n=1}^{\infty}f_{mn}^2\left[D_x\left(\frac{m^2\pi^2}{a^2}\right)^2+D_y\left(\frac{n^2\pi^2}{b^2}\right)^2+(D_{xy}+D_{yx})\frac{m^2n^2\pi^4}{a^2b^2}+4G_p\frac{m^2n^2\pi^4}{a^2b^2}\right]}{\displaystyle\sum_m\sum_n\sum_p\sum_q f_{mn}f_{pq}\frac{mnpq}{(m^2-p^2)(q^2-n^2)}} \tag{25}$$

Differentiating eqn (25) by each coefficient f_{mn} and setting this equal to zero in order to minimize the absolute value of ${}_{cr}N_{xy}$, homogeneous linear equations for f_{mn} are obtained. These equations are divided into two groups. One is that for symmetrical mode ($m+n$ = even number), and the other is that for antisymmetrical mode ($m+n$ = odd number) about the center of the plate. ${}_{cr}N_{xy}$ is obtained by the process of making zero the determinant of the coefficient matrix of each group of equation. And two solutions with $\pm$ signs are obtained. The smaller absolute value of ${}_{cr}N_{xy}$ between symmetrical and antisymmetrical mode is the significant solution to be obtained. ${}_{cr}N_{xy}$ is calculated by means of iteration to increase the assumed stress step by step starting from low value in order to find out the stress at which the sign of the determinant changes.

The degrees of m and n are selected to five respectively, and the combination of (m, n) is 25. In these, combination for symmetrical mode is 13 and that for antisymmetrical mode is 12.

Elastic analysis by these degrees gives almost the same solution as Seydel's (1933) precise one for $\alpha=1$.

The bending stiffnesses are elastic and are given by eqn (11) in the both plastic flow and strain hardening ranges. The shear modulus are given by eqns (14), (15) in the plastic flow and strain hardening ranges, respectively. The differences of the solution between the following two cases is only small. One is the analysis by the use of sectional stiffnesses in

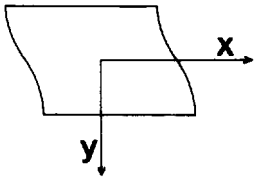

Fig. 4. x, y axes of plate for $\alpha = \infty$.

the plastic flow range, and the other is the analysis by the use of those in the strain hardening range. The difference is largest for $\alpha = 1$, and is at most 1.4%. Therefore the plastic buckling of the steel plates in shear has been analyzed using moduli expressed by the eqns (11) and (14).

(b) When $\alpha = \infty$.

When $\alpha = \infty$, Southwell and Skan (1924), as mentioned before, had obtained precise buckling stress together with the mode (buckling wave) in the elastic analysis. They had made clear that the mode had resulted in harmonic function toward the longitudinal direction. Therefore, the same mode is assumed for the plastic analysis in this case. Thus, I obtain

$$w = d\cos\left(\frac{\pi}{\lambda}x - \psi\right) \tag{26}$$

where

d = function of y which determines the magnitude of buckling wave

λ = half wave length in the longitudinal direction

ψ = function of y.

Figure 4 shows the direction of x- and y-axes with an origin at the center of one half wave in the longitudinal direction of the plate. It is unnecessary to analyze an anti-symmetrical mode because it appears as a part of sequential symmetrical mode and its buckling strength is equivalent to that of a symmetrical mode.

Equation (26) is transformed to

$$w = d\cos\frac{\pi}{\lambda}x\cos\psi + d\sin\frac{\pi}{\lambda}x\sin\psi \tag{27}$$

Replace the moduli in the above equation as follows

$$\left.\begin{aligned} d\sin\psi &= h_1(y) \\ d\cos\psi &= h_2(y) \end{aligned}\right\} \tag{28}$$

h_1 and h_2 must satisfy the following boundary conditions in the simply supported case. at $y = \pm h/2$

$$\left.\begin{aligned} h_i &= 0 \\ \frac{\partial^2 h_i(y)}{\partial y^2} &= 0 \\ (i &= 1 \text{ or } 2) \end{aligned}\right\} \tag{29}$$

Because the buckling mode is symmetrical, each function must be expressed by the following Fourier series to satisfy the above boundary conditions.

$$\left.\begin{aligned} h_1(y) &= \sum_{m=1}^{\infty} f_m \sin\frac{2m\pi}{b}y \\ h_2(y) &= \sum_{n=1}^{\infty} g_n \cos\frac{(2n-1)\pi}{b}y \end{aligned}\right\} \tag{30}$$

Therefore

$$\left.\begin{aligned} w = &\sum_{m=1}^{\infty} f_m \sin\frac{2m\pi}{b}y \sin\frac{\pi}{\lambda}x \\ &+ \sum_{n=1}^{\infty} g_n \cos\frac{(2n-1)\pi}{b}y \cos\frac{\pi}{\lambda}x \end{aligned}\right\} \tag{31}$$

The buckling strength is obtained applying eqn (31) into eqn (21) and eqn (23) which express the strain energy and the work of external forces respectively. The ranges to integrate are

$$-\frac{b}{2} \leqslant y \leqslant \frac{b}{2}, \qquad -\frac{\lambda}{2} \leqslant x \leqslant \frac{\lambda}{2}$$

We obtain the following strain energy V

$$V = \tfrac{1}{2} I A_1 \tag{32}$$

$$\begin{aligned} A_1 = {} & D_x \frac{\lambda b}{4}\left(\frac{\pi}{\lambda}\right)^4 \sum_{m=1}^{\infty}\sum_{n=1}^{\infty}\left(f_m^2 + g_n^2\right) \\ & + D_y \frac{\lambda b}{4}\left(\frac{\pi}{b}\right)^4 \sum_{m=1}^{\infty}\sum_{n=1}^{\infty}\left[(2m)^4 f_m^2 + (2n-1)^4 g_n^2\right] \\ & + (D_{xy} + D_{yx}) \frac{\lambda b}{4}\frac{\pi^4}{(b\lambda)^2} \sum_{m=1}^{\infty}\sum_{n=1}^{\infty}\left[(2m)^2 f_m^2 + (2n-1)^2 g_n^2\right] \\ & + 4G_p \frac{\lambda b}{4}\frac{\pi^4}{(b\lambda)^2} \sum_{m=1}^{\infty}\sum_{n=1}^{\infty}\left[(2m)^2 f_m^2 + (2n-1)^2 g_n^2\right] \end{aligned} \tag{33}$$

The work T of external forces is expressed by

$$T = {}_{cr}N_{xy}\pi B_1 \tag{34}$$

$$B_1 = \sum_{m=1}^{\infty}\sum_{n=1}^{\infty}(-1)^{(m-n)}\frac{4m(2n-1)}{(2m)^2-(2n-1)^2} f_m g_n \tag{35}$$

Equating eqn (32) to eqn (34) the following ${}_{cr}N_{xy}$ is obtained

$${}_{cr}N_{xy} = \frac{I}{2\pi B_1} A_1 \tag{36}$$

Differentiating the above eqn (36) by each modulus and set equal to zero in order to satisfy the condition to minimize ${}_{cr}N_{xy}$, the homogeneous linear equations for f_m and g_n are obtained. Therefore the buckling strength ${}_{cr}N_{xy}$ is determined as the absolute value which makes the determinant of coefficient matrix of these equations zero.

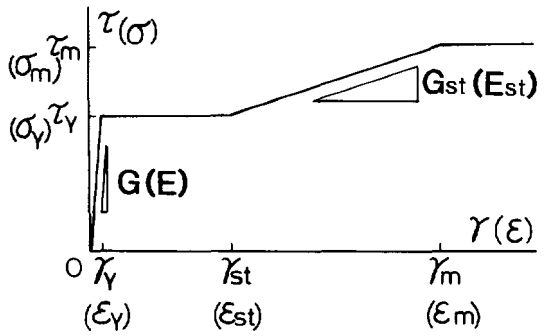

Fig. 5. Stress strain relation.

Each degree of m and n is selected to be 6. Accuracy of the analysis by these degrees has been confirmed in the elastic case for long plate. The discrepancy between this solution and exact value by Southwell and Scan (1924) has been at most 0.9%.

3.3. *Analytical results in the plastic range*

In the analysis of plastic buckling stress of steel plates in shear, the constant bending stiffnesses (eqn (11)) and shear modulus (eqn (14)) obtained before in the plastic flow range are applied to the whole plastic range. The buckling stress is described in the style of eqn (16). Here K_e in eqn (16) is exchanged by K_p in the plastic range. Therefore

$$\tau_{cr} = \frac{\pi^2 E}{12(1-\nu^2)} \left(\frac{t}{b}\right)^2 K_p \tag{37}$$

The value of coefficient K_p is analytically obtained taking α as a parameter. Buckling strain is obtained as the point on the shear stress–strain curve. This curve is shown as the following.

The material is mild steel SS400 in Japan Industrial Standard. The ideally assumed typical shear stress–strain curve is drawn in Fig. 5 in correspondence with uniaxial tension curve. This curve consists of elastic, plastic flow and strain hardening ranges having the following maximum plateau. The characteristic values, which define this curve, are assumed as Table 1. In this table, the following symbols are used:

σ_Y = yield stress in uniaxial tension
σ_m = maximum stress in uniaxial tension
ε_Y = yield strain in uniaxial tension
ε_{st} = strain at the onset of strain hardening in uniaxial tension ($=11\varepsilon_Y$)
ε_m = strain at maximum stress in uniaxial tension
E_{st} = tangent modulus in the strain hardening range in uniaxial tension ($=1/33E$)
τ_Y = yield shear stress
τ_m = maximum shear stress
γ_Y = yield shear strain
γ_{st} = shear strain at the onset of strain hardening
γ_m = shear strain at maximum shear stress

Table 1. Material property

σ_Y (N mm^{-2})	σ_m (N mm^{-2})	ε_Y (%)	ε_{st} (%)	ε_m (%)	E (N mm^{-2})	E_{st} (N/mm^2)
235	353	0.11	1.26	3.15	2.06×10^5	6.237×10^3
τ_Y (N mm^{-2})	τ_m (N mm^{-2})	γ_Y (%)	γ_{st} (%)	γ_m (%)	G (N mm^{-2})	G_{st} (N/mm^2)
118	177	0.15	1.86	4.68	7.9×10^4	2.089×10^3

Table 2. Value of K_p

α	0.5	1.0	1.2	1.4	1.5	1.6
mode	A	S	S	S	S	S
K_p	18.6	6.22	5.41	5.11	5.05	5.02
α	1.8	2.0	2.5	3.0	4.0	∞
mode	A	A	A	S	S	S & A
K_p	4.93	4.66	4.40	4.33	4.23	3.96

G_{st} = tangent modulus in the strain hardening range in shear.
τ_Y is expressed by the following equation using σ_Y based on Tresca yield criterion.

$$\tau_Y = \frac{1}{2}\sigma_Y \tag{38}$$

τ_m is obtained by the following equation, which assuming the similar relation as that in yield stresses, holds good for maximum stresses.

$$\tau_m = \frac{1}{2}\sigma_m \tag{39}$$

The length of yield plateau γ_0 is estimated by $\mathrm{d}\gamma^p_{max}$ in eqn (2). In the right side of eqn (2), the length of yield plateau ε_0 in uniaxial tension is substituted for $\mathrm{d}\varepsilon^p_x$. Therefore

$$\gamma_0 = \frac{3}{2}\varepsilon_0 \tag{40}$$

where

$$\gamma_0 = \gamma_{st} - \gamma_Y$$
$$\varepsilon_0 = \varepsilon_{st} - \varepsilon_Y$$

Therefore

$$\gamma_{st} = \gamma_Y + \gamma_0 \tag{41}$$

In Table 1,
γ_{st} is calculated by eqns (40) and (41) equating ε_0 to $10\varepsilon_Y$.
G_{st} is given by G_p in eqn (15) substituting E_{st} for E_t on the right side of this equation.

3.3.1. *Buckling stress.* The values of K_p in eqn (37) are shown in Table 2 and Fig. 6 taking α as a parameter. These values in Table 2 give the smaller ${}_{cr}N_{xy}$ between symmetrical and antisymmetrical modes. When $\alpha = \infty$, the value of λ which gives the smallest value of ${}_{cr}N_{xy}$ is $1.09b$. In the mode column of this table, S means a symmetrical mode and A means an antisymmetrical one. Figure 6 illustrates the coefficient K_p taking $1/\alpha$ as abscissa for $0 \leqslant 1/\alpha \leqslant 1$. In this figure, a one-dotted chain line is drawn by approximately eqn (17) for K_e and a solid line is the value of K_p whose two modes are distinguished by symbols S and A, respectively. The value of K_p shows a tendency to increase when $1/\alpha$ decreases near zero neighborhood. This results from the approximate analysis which regards the plate length as definite and applies definite number of Fourier series to their buckling modes. But as $1/\alpha$ approaches zero, the value of K_p must get closer and closer to that for $\alpha = \infty$ (point M in Fig. 6).

A broken line is the approximate equation as follows. Namely, this curve is obtained by assuming a parabola which passes two points M and N corresponding to $\alpha = \infty$ and 1

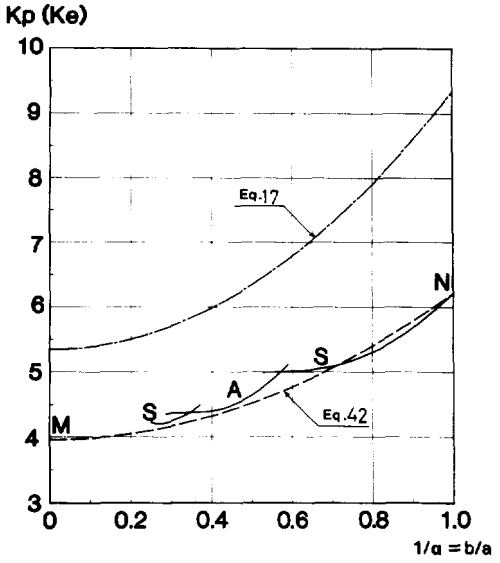

Fig. 6. Value of $K_p(K_c)$

respectively. Thus we obtain

$$K_p = 3.96 + 2.24\left(\frac{1}{\alpha}\right)^2 \tag{42}$$

(apply for $\alpha \geqslant 1$).

This parabola is somewhat smaller than the value analytically obtained, but is higher about 3% near $1/\alpha = 0.85$.

For the range $\alpha < 1$, there is the same conversion for K_p as the elastic case (eqn (18) and (19)). Therefore we obtain

$$K_p = 2.24 + 3.96\left(\frac{1}{\alpha}\right)^2 \tag{43}$$

(apply for $\alpha < 1$).

The buckling curve is generally represented as Fig. 7. The ordinate is the buckling stress τ_{cr} and the abscissa is width-to-thickness ratio b/t. $A \sim B$ is an elastic buckling curve and $C \sim D$ is a plastic buckling curve over yield stress. $B \sim C$ is the range in which the buckling is caused at the yield stress. The upper limit of this curve is determined by the

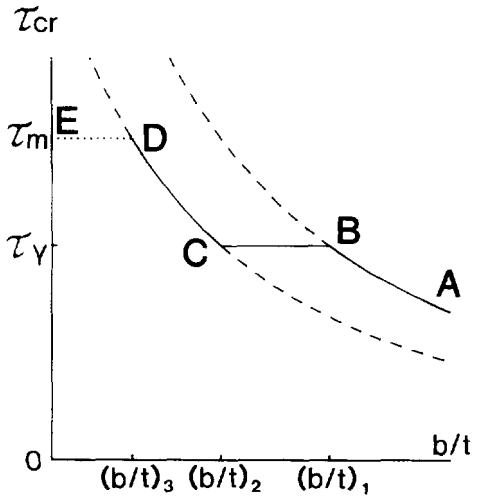

Fig. 7. Buckling curve.

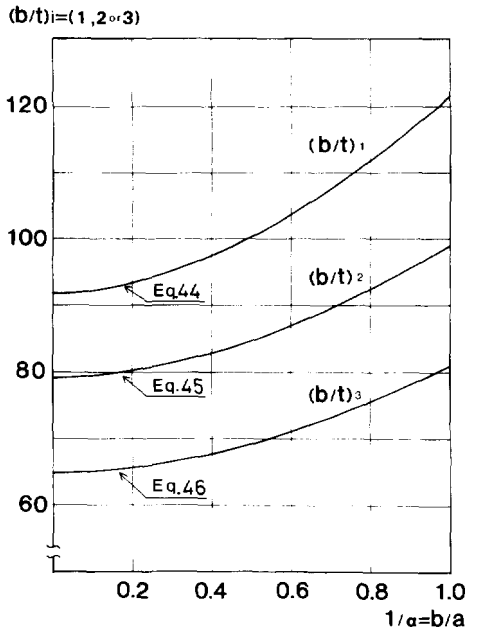

Fig. 8. Value of $(b/t)_i$ $(i = 1, 2 \text{ or } 3)$.

maximum shear stress τ_m in the material property, Fig. 5. $(b/t)_1$, $(b/t)_2$ and $(b/t)_3$ correspond to the points B, C and D in Fig. 7, respectively. Based on the material property, Fig. 5, the plates with b/t smaller than $(b/t)_3$ reach τ_m without following buckling.

The values of $(b/t)_1$, $(b/t)_2$ and $(b/t)_3$ are calculated by the following equations with a parameter α by the use of K_e (eqn (17) and (19)) and K_p (eqn (42) and (43)). Their values are shown in Fig. 8 for $\alpha \geqslant 1$.

When $\alpha \geqslant 1$

$$\left(\frac{b}{t}\right)_1 = \sqrt{\frac{\pi^2 E}{12(1-\nu^2)\tau_Y}\left[5.34+4.0\left(\frac{1}{\alpha}\right)^2\right]} \tag{44}$$

$$\left(\frac{b}{t}\right)_2 = \sqrt{\frac{\pi^2 E}{12(1-\nu^2)\tau_Y}\left[3.96+2.24\left(\frac{1}{\alpha}\right)^2\right]} \tag{45}$$

$$\left(\frac{b}{t}\right)_3 = \sqrt{\frac{\pi^2 E}{12(1-\nu^2)\tau_m}\left[3.96+2.24\left(\frac{1}{\alpha}\right)^2\right]} \tag{46}$$

When $\alpha < 1$

$$\left(\frac{b}{t}\right)_1 = \sqrt{\frac{\pi^2 E}{12(1-\nu^2)\tau_Y}\left[4.0+5.34\left(\frac{1}{\alpha}\right)^2\right]} \tag{47}$$

$$\left(\frac{b}{t}\right)_2 = \sqrt{\frac{\pi^2 E}{12(1-\nu^2)\tau_Y}\left[2.24+3.96\left(\frac{1}{\alpha}\right)^2\right]} \tag{48}$$

$$\left(\frac{b}{t}\right)_3 = \sqrt{\frac{\pi^2 E}{12(1-\nu^2)\tau_m}\left[2.24+3.96\left(\frac{1}{\alpha}\right)^2\right]} \tag{49}$$

Table 3. Value of $(b/t)_i$ ($i = 1$, 2 or 3)

α	$(b/t)_1$	$(b/t)_2$	$(b/t)_3$
0.5	200.3	169.1	138.1
1.0	121.5	99.0	80.9
1.5	106.1	88.5	72.3
2.0	100.1	84.6	69.0
∞	91.9	79.1	64.6

These values for the specific values of $\alpha(=0.5, 1.0, 1.5, 2.0$ and $\infty)$ are listed in Table 3.

Figure 9 is a buckling curve for $\alpha = \infty$. In this figure (A) is an elastic buckling curve and (B) is a plastic buckling curve obtained by the present paper. The values of $(b/t)_1$, $(b/t)_2$ and $(b/t)_3$ defined in Fig. 7 are written concretely in this figure. The solutions by the secant modulus method (Gerard, 1948) and the deformation theory (Stowell, 1949) are very low and are beyond the boundary of Fig. 9.

3.3.2. *Buckling strain.* The buckling strain is generally expressed in Fig. 10. The ordinate is buckling strain γ_{cr} and the abscissa is width-to-thickness ratio b/t. The symbols A, B, C and D correspond to those on the buckling stress curve in Fig. 7. The point C in Fig. 7 lies on both yield plateau and strain hardening curve. Thus the plate at this point is just situated at a limit at which the buckling strain translates from γ_Y and γ_{st}. Therefore one point C on the buckling stress curve corresponds to two points Cs on the buckling strain curve. The plates with width-to-thickness ratio smaller than that at the point D reach γ_m

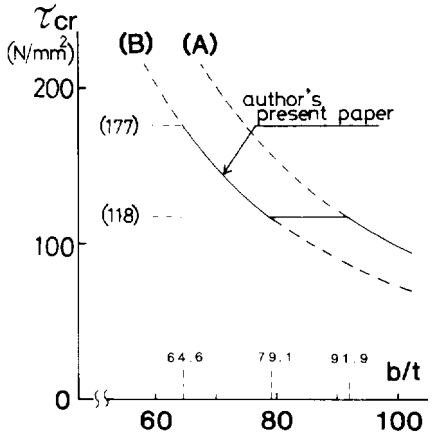

Fig. 9. Buckling curve for $\alpha = \infty$.

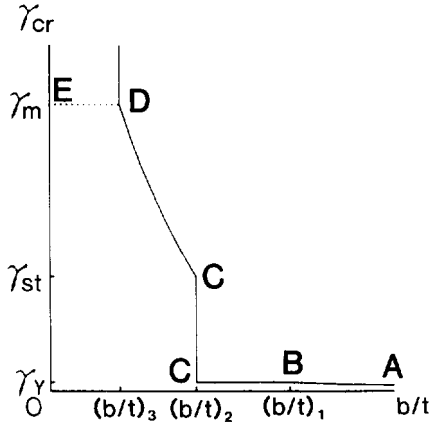

Fig. 10. Buckling strain.

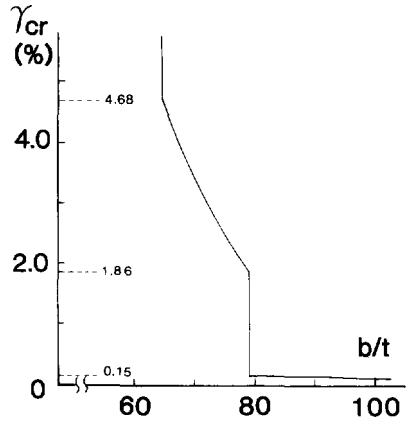

Fig. 11. Buckling strain for $\alpha = \infty$.

and thereafter the strain progresses along the material property without experience of buckling. The buckling strain curve is drawn in Fig. 11 for $\alpha = \infty$ specifically. This curve corresponds to the buckling stress curve in Fig. 9.

3.3.3. *Mode of buckling wave.* The mode of buckling wave analytically obtained is shown in Fig. 12-1–3. As the representative of plates with finite length, $\alpha = 1$ and 2 are selected. The former shows a symmetrical mode and the latter shows an antisymmetrical mode. Each mode is expressed by contour lines setting the maximum deformation w_{max} equal to 1.

4. TEST AND ANALYTICAL RESULTS

A shear test of *H*-shaped steel cantilever was conducted by the author (Inoue and Akiyama, 1985).

4.1. *Test program*

The specimens are welded *H*-shaped cantilever as shown in Fig. 13. After completion of welding the specimens were not annealed.

The material of the cantilever is mild steel designated by SS400 in JIS. The measured thickness of the web plate elements was 4.44 mm. The measured dimensions of the specimens are shown in Table 4. The total number of the specimens is 5. The aspect ratio α of the specimens is 2. The flange thickness is varied for each specimen so as to avoid the premature yielding of the flange plate before the shear yielding of the web plate.

The definition of symbols in Table 4 is as follows:

d: width of the web

$2c$: width of the flange

t_w: thickness of the web

t_f: thickness of the flange

l: length of the specimen

d/t_w: width-to-thickness ratio of the web

c/t_f: width-to-thickness ratio of the half flange

The mechanical property of the web plate from tension test is shown in Fig. 14 and Table 5. The definition of symbols in the figure and table is quite the same as defined in Table 1 except that symbol "*e*", which means that they are experimentally obtained, is attached in addition to the original symbols. The length of the yield plateau of this material is shortish as compared with ordinary mild steel.

4.2. *Test procedure*

Shear load Q was monotonically and horizontally applied to the top of the specimen using 200-ton actuator, and the base of the specimen was fixed to the floor as Fig. 13. The

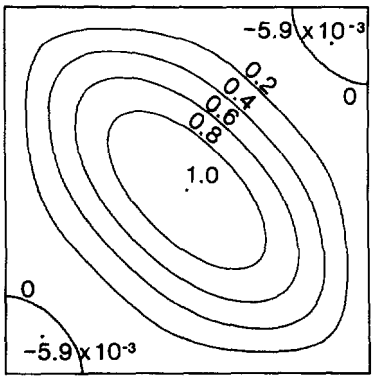

Fig. 12-1. Buckling mode for $\alpha = 1$.

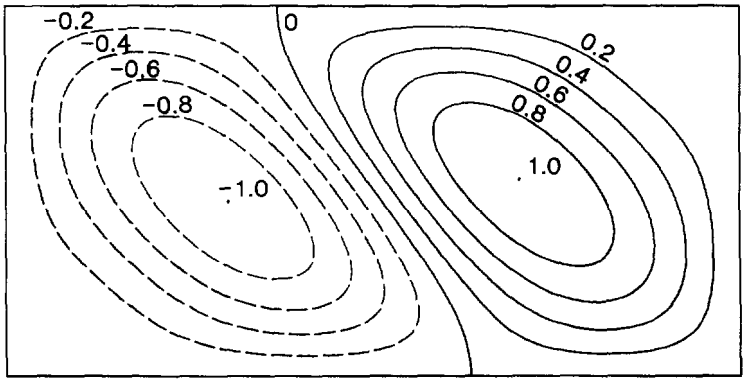

Fig. 12-2. Buckling mode for $\alpha = 2$.

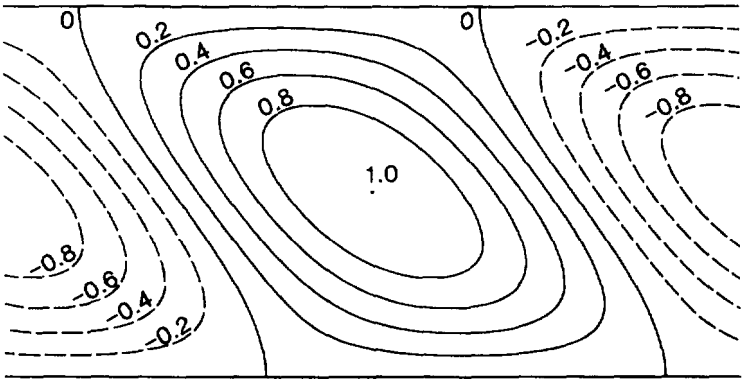

Fig. 12-3. Buckling mode for $\alpha = \infty$.

horizontal displacement δ of the top of the specimen was measured, and the shear deformation angle θ was calculated by $\theta = \delta/l$ as Fig. 13.

4.3. *Test results*

4.3.1. *Load-deformation relation.* $Q/{}_eQ_Y - \theta/{}_e\theta_Y$ relations were obtained as test results. These are relations between the following two nondimensionalized volumes. One is working shear load Q divided by the yield shear load ${}_eQ_Y$, and the other is shear deformation angle θ divided by ${}_eQ_Y \cdot {}_eQ_Y$ is the load just at the point of intersection of the following two straight lines. One is the elastic inclination line, which includes both shear and bending components of deformation, and the other is the straight line, which represents the increasing part of strain hardening range on the load-deformation curve. ${}_e\theta_Y$ is calculated diving

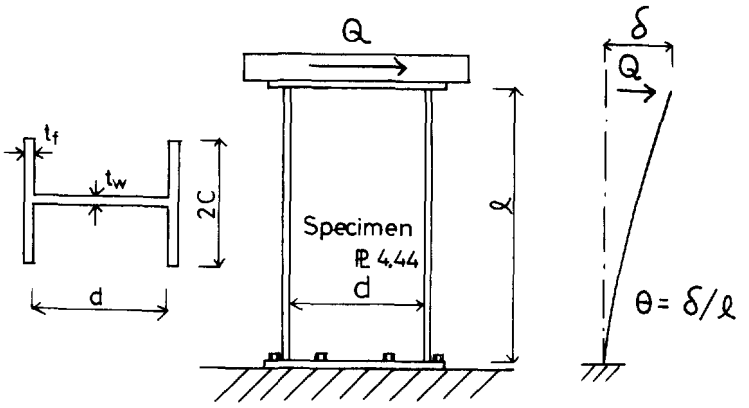

Fig. 13. Specimens.

Table 4. Dimensions of specimens

Code	d (mm)	$2c$ (mm)	t_w (mm)	t_f (mm)	d/t_w	c/t_f	l (mm)	l/d
2D-30	135	171	4.44	8.56	30.4	10.0	270	2.0
40	180	168	4.44	11.74	40.5	7.2	360	2.0
50	225	204	4.44	11.74	50.7	8.7	450	2.0
60	270	176	4.44	15.36	60.8	5.7	540	2.0
70	315	208	4.44	15.36	71.0	6.8	630	2.0

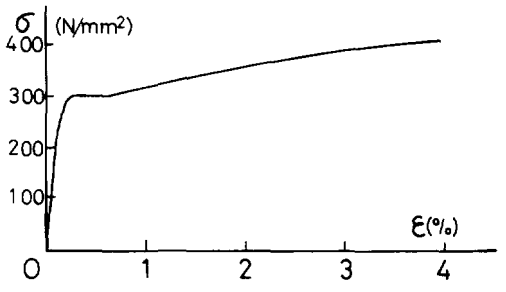

Fig. 14. Stress–strain curve of web plate from tension test.

Table 5. Material property of the web plate from tension test

${}_e\sigma_Y$ (N/mm²)	${}_e\sigma_m$ (N/mm²)	${}_e\varepsilon_Y$ (%)	${}_e\varepsilon_{st}$ (%)	${}_eE$ (N/mm²)	${}_eE_{st}$ (N/mm²)
295	469	0.143	0.49	205940	4315

${}_eQ_Y$ by the elastic stiffness of the member. Nondimensionalized load-deformation curves are shown in Fig. 15.

4.3.2. *Stress increase and analytical value.* Nondimensionalized stress increase rate ρ, or the experimentally obtained maximum load Q_m divided by ${}_cQ_Y$, are shown in Table 6. These are graphically shown in Fig. 16. In Fig. 16, the ordinate is the stress increase rate ρ, and the abscissa is equivalent to the width-to-thickness ratio $d/t_w\sqrt{{}_e\gamma_Y \cdot {}_e\gamma_Y}$ is the yield shear strain, and is a half of ${}_e\sigma_Y$ divided by elastic shear modulus G.

We compare these ρs with the analytical values obtained in Section 3. For comparison, eqn (37) in Section 3 is used taking 3.96 for K_p, which is the lowest value for long plate.

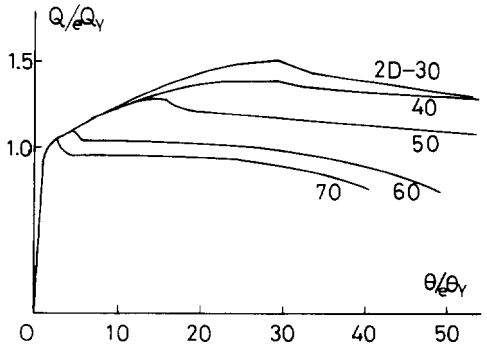

Fig. 15. Test results.

Table 6. Test results

Code	ρ	$d/t\sqrt{\gamma_Y}$
2D-30	1.52	1.31
40	1.40	1.75
50	1.29	2.19
60	1.10	2.62
70	1.05	3.06

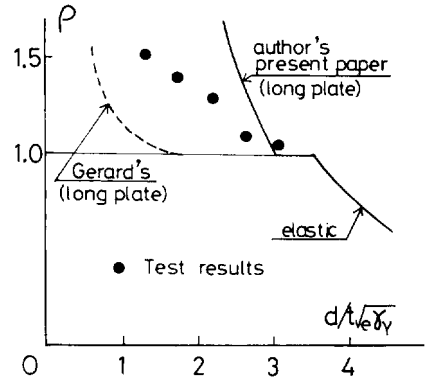

Fig. 16. Stress increase rate and analytical value.

$$\frac{\tau_{cr}}{\tau_Y} = \frac{\pi^2}{6(1-\nu)} K_p \frac{1}{(b/t\sqrt{\gamma_Y})^2} \tag{50}$$

Supposing the left-hand side of the above equation is equal to ρ, and putting b/t and γ_Y equal to d/t and $_e\gamma_Y$, respectively, this equation is drawn by a solid line in Fig. 16.

For comparison, the solutions by Gerard (1948), which used secant modulus method, are also drawn in Fig. 16 by a dashed line. This curve is derived for the long plates simply supported along all four edges. These solutions are expressed by the following simple equation.

$$\tau_{cr} = \frac{G_s}{G} \frac{\pi^2 K_c E}{12(1-\nu^2)} \left(\frac{t}{b}\right)^2 \tag{51}$$

where

G_s: secant modulus in shear

K_c: 5.34 when the plate is sufficiently long.

There is only a slight different between the solutions by Grerard (1948) and the solutions of deformation theory by Stowell (1949) and Bijlaard (1949). Therefore a dashed line in Fig. 16 is considered to be representative of past analytical investigations.

This figure demonstrates that the analysis and experiment have good agreement with respect to the upper limit of the width-to-thickness ratio range in which shear stress can be increased over the yield shear stress into the strain hardening range.

With the decrease in the effective width-to-thickness ratio in the strain hardening range, the stress increase rate becomes larger, but the experimental data points are below the analytical predictions. The reason for this discrepancy is not apparent, but may be due to the loss of geometric similarity of the yield locus in the strain hardening range, which is the basic assumption in this analysis. When the geometric similarity is impaired, slip deformations in different directions can be combined.

It can be concluded that the proposed analytical method provides a good agreement with the experimental results especially in the early plastic zone.

5. CORRESPONDENCE TO PAST DESIGN FORMULAS

Kato (1979) gave the following empirical formula for the limit value of width-to-thickness ratio which enabled the buckling stress to reach the yield shear stress by the analogy of column buckling.

$$\frac{b}{t} \leqslant \frac{114}{\sqrt{\sigma_Y}} \tag{52}$$

This formula could be obtained from elastic buckling stress curve of infinitely long simply supported plate. Its method was to draw a tangent line at $0.6\tau_Y$ on the elastic buckling stress curve and to determine a point at which the line reached τ_Y.

Equation (52) was later simplified on the safety side, as the following formula and was adopted in a specification (1983) by Architectural Institute of Japan.

$$\frac{b}{t} \leqslant \frac{110}{\sqrt{\sigma_Y}} \tag{53}$$

The limit values of width-to-thickness ratio by eqn (52) and (53) are 73.6 and 71.0 respectively for the mild steel, JIS-SS400. the limit value of width-to-thickness ratio $(b/t)_2$, which enable the plate to reach the onset of strain hardening, by the author's analysis is 79.1 as Fig. 9 for the same condition as Kato's formulas were derived. This limit value by the author is a little larger than that by Kato's formula (52).

6. SUMMARY AND CONCLUSIONS

(1) On the basis of the Tresca yield criterion and assuming that the plastic deformation is generated by planar slip in the direction of the maximum shear stress, the bending and torsional stiffnesses of the yielded steel plates in shear were derived.
(2) All the bending stiffnesses take the elastic values in both plastic flow and strain hardening ranges.
(3) The torsional stiffness is zero in the plastic flow range. In the strain hardening range, it is equal to $G_{st}I$. G_{st} is shown in Table 1 for mild steel, JIS-SS400.
(4) The contribution of G_{st} to the buckling stress is very small, e.g. at most 1.4% for $\alpha = 1$.
(5) Mild steel, JIS-400, is selected as a standard structural material for an example of buckling analysis. Standard buckling curves both for stress and strain were derived.
(6) A shear test of H-shaped steel cantilever was conducted for comparison with the analysis from the view point of stress increase.
(7) The analytically obtained width-to-thickness ratio to reach the onset of strain hardening coincides with the test result.

(8) With the decrease in the effective width-to-thickness ratio in the strain hardening range, the stress increase rate obtained experimentally is below the analytical predictions.

REFERENCES

Architectural Institure of Japan (1970). Specification for Design of Steel Structures (in Japanese).

Bijlaad, P. P. (1949). Theory and test on the plastic stability of plates and shells. *J. Aero. Sci.* **16,** 529–541.

Bleich, H. (1952). *Buckling Strength of Metal Structures*, p. 395. McGraw-Hill, New York.

Gerard, G. (1948). Critical shear stress of plates above the proportional limit. *J. Appl. Mech.* **15**(1), 7–12.

Inoue, T. and Akiyama, H. (1985). Load-deformation relationship of shear-yielding type H-section steel numbers. *J. Structure Const. Engng (Trans. AIJ)* **348,** 52–60 (in Japanese).

Inoue, T. and Kato, B. (1993). Analysis of plastic buckling of steel plates. *Int. J. Solids Structures* **30**(6), 835–856.

Inoue, T. (1994). Analysis of plastic buckling of rectangular steel plates supported along their four edges. *Int. J. Solids Structures* **31**(2), 219–230.

Kato, B. (1979). *Steel Structures*. Series 18, Outline of Structures in Architecture. Shokokusha, Tokyo (in Japanese).

Reuss, A. (1930). *Zeits. ang. Math. Mech.* **10,** 266.

Sewell, M. J. (1973). A yield-surface corner lowers the buckling stress of an elastic-plastic plate under compression. *J. Mech. Phys. Solids* **21,** 19–45.

Sewell, M. J. (1974). A plastic flow rule at a yield vertex. *J. Mech. Phys. Solids* **22,** 469–490.

Seydel, E. (1933). Uber das ausbelen von rechteckigen isotropen oder orthogonal-anisotropen platter bei schub-beanspruchung. *Ingenieur Archiv.* **4,** 169.

Shanley, F. R. (1947). Inelastic column theory. *J. Aero. Sci.* **14**(5), 261–267.

Skan, S. W. and Southwell, R. V. (1924). On the stability under shearing forces of a flat elastic strip. *Proc. Roy. Soc. (London)*, Series A, **105,** 582.

Stein, M. and Neff, J. (1947). Buckling stress of simply supported rectangular flat plates in shear. *NACA Tech. Note* 1222.

Stowell, E. Z. (1948). A unified theory of plastic buckling of columns and plates. *NACA Tech. Note* 1556.

Stowell, E. Z. (1949). Critical shear stress of infinitely long plates in the plastic region. *NACA Tech. Note.* 1681.

Timoshenko, S. P. and Gere, J. M. (1961). *Theory of Elastic Stability*. McGraw-Hill, New York.

APPENDIX: DIFFERENCE BETWEEN THE AUTHOR'S ANALYSIS AND THAT OF INCREMENTAL THEORY

The solution of plastic shear buckling stress by the incremental theory is exactly the same as author's analysis except that yield shear stress differs from the author's one. In the incremental theory associated with the von Mises yield criterion, the yield shear stress is $\sigma_y/\sqrt{3}$ and therefore is higher about 16% than that used in this paper. Thus the buckling curve in Fig. 9 is efficient also for the incremental theory if the yield plateau only is enhanced. The reason why the drastic reduction of plastic buckling stress, or uniaxial compression, can't be brought about in shear analytically compared with the incremental theory is that the yield point, on the biaxially expressed the Tresca yield locus by principal stresses, has no corner. Furthermore, there is a specific character for the bending and torsional stiffnesses that these values are decided by the inclination of the tangent on the yield locus. There is no difference between two inclinations of the tangent at the yield points on the two yield locuses, one of which is based on the Tresca yield criterion and the other of which is based on the von Mises yield criterion. In order to prove the above feature, it is quite sufficient to show the agreement of the values of bending and torsional stiffnesses brought about by the incremental theory with the author's one.

(Incremental theory)

(a) Plastic flow range

The incremental stress–strain theory in the plastic flow range was given by Reuss (1930) on the basis of von Mises yield criterion as follows:

$$\mathrm{d}\varepsilon'_{ij} = \frac{\mathrm{d}\sigma'_{ij}}{2G} + \sigma'_{ij}\,\mathrm{d}\lambda \tag{A1}$$

where $\mathrm{d}\lambda$ = a constant of proportionality.

Tensor notations used are: subscript ij for stress and strain means that, $\sigma_{11} = \sigma_x$, $\sigma_{22} = \sigma_y$, $\sigma_{33} = \sigma_z$, $\sigma_{12} = \tau_{xy}$, $\sigma_{23} = \tau_{yz}$, $\sigma_{31} = \tau_{zx}$ and $\varepsilon_{11} = \varepsilon_x$, $\varepsilon_{22} = \varepsilon_y$, $\varepsilon_{33} = \varepsilon_z$, $\varepsilon_{12} = \frac{1}{2}\gamma_{xy}$, $\varepsilon_{23} = \frac{1}{2}\gamma_{yz}$, $\varepsilon_{31} = \frac{1}{2}\gamma_{zx}$, respectively. σ'_{ij} and ε'_{ij} are deviatoric stress and deviatoric strain respectively [for example, $\sigma'_x = \sigma_x - \frac{1}{3}(\sigma_x + \sigma_y + \sigma_z)$].

When a plate is subjected to uniformly distributed in-plane pure shear stress under the plane-stress condition, it can be assumed that stresses all vanish except τ_{xy}. At the instant of buckling, bending and torsion of the plates will occur without strain reversal according to Shanley's tangent modulus concept, and the condition of no strain reversal is written as $\mathrm{d}J_2 = 0$, where $J_2 = \tau_{xy}^2$ = second invariant of deviatoric stress tensor for this particular case.

Namely

$$\mathrm{d}\tau_{xy} = 0 \tag{A2}$$

Under this stress condition, the stress–strain relationship by eqn (A1) is written in unabridged form

$$\left.\begin{aligned} d\varepsilon_x &= \frac{1}{E}(d\sigma_x - \nu\, d\sigma_y) \\ d\varepsilon_y &= \frac{1}{E}(d\sigma_y - \nu\, d\sigma_x \\ d\gamma_{xy} &= 2\tau_{xy}\, d\lambda \end{aligned}\right\} \tag{A3}$$

Equation (A3) perfectly agree with eqn (8) which is the base of the author's analysis if $2\tau_{xy}\,d\lambda$ is replaced with $d\kappa$. Therefore the bending and torsional stiffnesses perfectly agree with the author's one.

(b) Strain hardening range

The incremental stress–strain relationship was given by the following equation.

$$d\varepsilon'_{ij} = \frac{d\sigma'_{ij}}{2G} + F\frac{\partial f}{\partial \sigma_{ij}}\,df \tag{A4}$$

where

$$F = \frac{3}{4J_2}\left(\frac{1}{E_t} - \frac{1}{E}\right)$$

F = loading function with $f = J_2 = \tau_{xy}^2$ is applied. The condition of no strain reversal is written as $dJ_2 \geqslant 0$, or $d\tau_{xy} \geqslant 0$. Under this stress condition, the stress–strain relation eqn (A4) is written in unabridged form

$$\left.\begin{aligned} d\varepsilon_x &= \frac{1}{E}(d\sigma_x - \nu\, d\sigma_y) \\ d\varepsilon_y &= \frac{1}{E}(d\sigma_y - \nu\, d\sigma_x) \\ d\gamma_{xy} &= \left[\frac{1}{G} + 3\left(\frac{1}{E_t} - \frac{1}{E}\right)\right] d\tau_{xy} \end{aligned}\right\} \tag{A5}$$

Equation (A5) agrees perfectly with eqn (9) which is obtained by the author. Therefore the bending and torsional stiffnesses perfectly agree with the author's.